Investigation of Out-of-Time Peaks Observed in Tagger Hodoscope Time Spectra

Richard T. Jones
Department of Physics, University of Connecticut
richard.t.jones@uconn.edu
gluex-doc-7388

September 11, 2026

Abstract

Time spectra of the GlueX tagging counters relative to the machine RF normally consist of narrow peaks spaced every 4 ns associated with the RF structure of the CEBAF electron beam to Hall D. During the spring 2026 run period, additional peaks appeared in the time spectra for the tagger hodoscope, with intensity that varied from counter to counter. The most prominent side peaks were seen in the counters at the low-energy end of the hodoscope. These counters are normally turned off when running at the standard 11.7 GeV Gluex energy, but were turned on during the special 3.8 GeV low-energy spring 2026 run period, revealing these anomalous peaks. This note summarizes the study of these peaks, leading to their identification with direct interactions in the phototube window by out-of-plane post-bremsstrahlung electrons, or by their showers from the poles of the tagger spectrometer and walls of the exit vacuum chamber. Running at low energy exacerbates this background in the tagger due to the enlarged cone of emission of post-bremsstrahlung electrons. However, these peaks will also be present in the downstream region of the tagger hodoscope during regular GlueX running at 11.7 GeV, albeit as reduced intensities.

1 Introduction

The purpose of this study is to investigate the origin of a set of unexpected peaks in the time spectrum of certain counters in the tagger hodoscope. When the pulse time of detected electrons in a tagging counter is plotted relative to the radiofrequency (RF) strobe from the CEBAF accelerator, a uniform sequence of regularly spaced peaks is observed with a spacing equal to the pulse period of the Hall D electron beam, approximately 4.008 ns. An example of this is shown in Fig. 1 showing the spectrum taken from one of the columns of the tagger microscope (tagm) during a recent run 140543. The events used to produce this plot were triggered by an e^+, e^- coincidence in the pair spectrometer. The enhancement of the peaks near $t = 0$ indicate that sometimes the e^+, e^- pair is produced by a beam photon that was radiated (tagged) by the same electron that hit this tagging counter. The width of the timing peaks in this figure is dominated by the time resolution of the tagger. This time spectrum conforms with expectations for a tagged photon beam.

In the same general vicinity of the tagging spectrometer focal plane where the tagger microscope was located when the data in Fig. 1 were taken, there is second array of tagging counters called the tagger hodoscope. In contrast to the dense packing of the conpact array of scintillating fibers in the microscope, the hodoscope consists of a sparse array of individual scintillating tiles spaced out along the entire length of the focal plane. Differences in the geometry of these two arrays will be important later on in this study, so these details will be deferred to the section on interpretation of results. For the present purpose, it is sufficient to point out that these two detectors serve as redundant subsystems in GlueX event reconstruction. Both of them measure the time of tag electrons whose coincidence with events in the GlueX spectrometer allows offline reconstruction of the energy of the photon that produced the event. Fig. 2 shows a time spectrum taken from the same run 140543 for one of the counters in the tagger hodoscope (tagh) that is located in physical proximity to the microscope. The secondary peaks that appear about 1 ns earlier than the main peaks are unexpected.

They do not appear in all of the hodoscope counters. In some counters they are highly suppressed, as shown in Fig. 3, while in others they rival the main peaks in intensity, as shown in Fig. 4. Fig. 5 shows the relative intensity of the side peaks across the entire hodoscope as a function of counter number from upstream (counter 1, lowest energy electrons, highest energy tagged photons) to downstream (counter 272, highest energy electrons, lowest energy tagged photons). Notice that the counters with the most intense side peaks appear in the downstream end of the hodoscope, in the same region where the microscope was located for the run period under study. Fig. 6 shows the same thing for the tagger microscope. None of the microscope channels show any clear evidence of these side peaks.

What is the origin of these side peaks? Do these electrons tag photons that reach the liquid hydrogen target and produce interactions that can satisfy the GlueX physics trigger? If so then they need to be included as legitimate tags in forming hypotheses for event reconstruction. If not, special care is needed to make sure that they get subtracted as accidentals so they do not bias the flux normalization for cross section measurements.

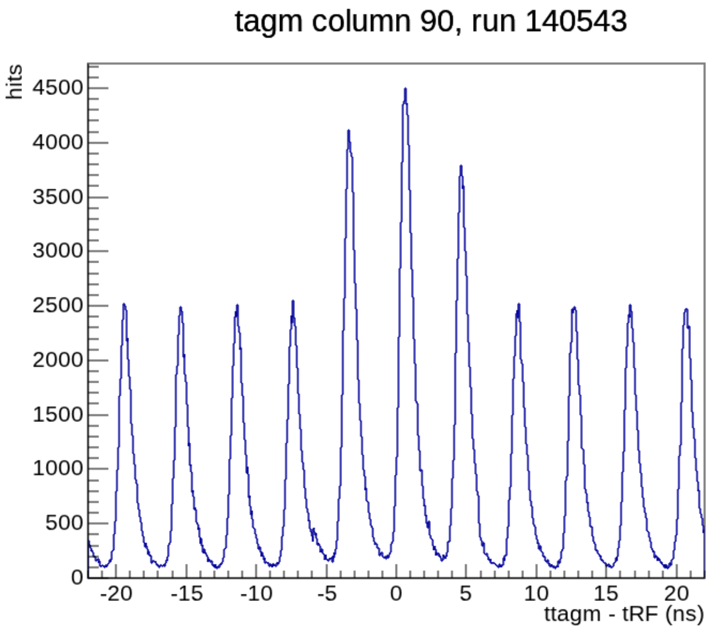

Figure 1: Tag electron hit time distribution relative to the accelerator RF clock for microcope column 90 measured during run 140543 in May, 2026. The enhancement of the three central RF buckets comes from true coincidences with the pair spectrometer located in the bremsstrahlung photon beam downstream of the tagger, which served as the trigger source for the events shown in this plot. The width and shape of the peaks comes almost entirely from the time resolution of the microscope.

2 Associating peaks with RF beam buckets

The most straight-forward interpretation of the side peaks in Fig. 2 is that they are caused by electrons that reach the tagging counters about 1 ns before the post-bremsstrahlung electrons in

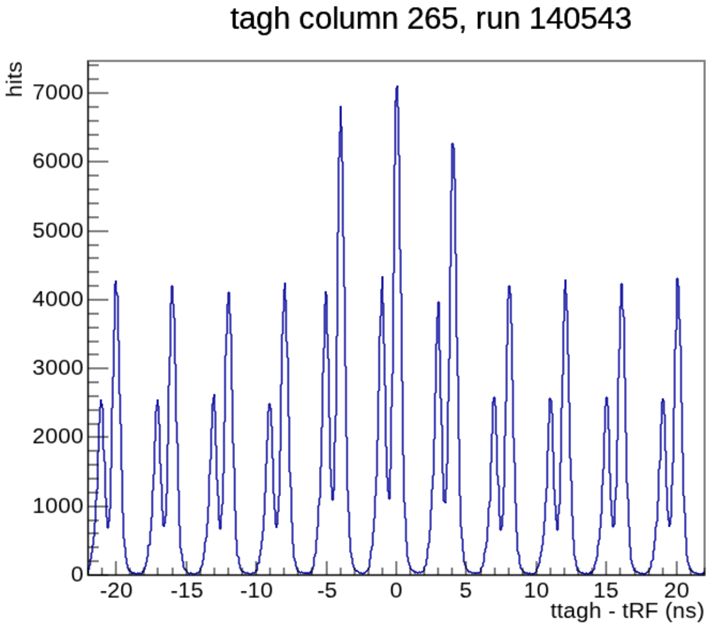

Figure 2: Tag electron hit time distribution relative to the accelerator RF clock for hodoscope counter 265 measured during run 140543 in May, 2026. The enhancement of the three central RF buckets comes from true coincidences with the pair spectrometer located in the bremsstrahlung photon beam downstream of the tagger, which served as the trigger source for the events shown in this plot. The width of the peaks comes almost entirely from the time resolution of the hodoscope, which is somewhat better than the microscope.

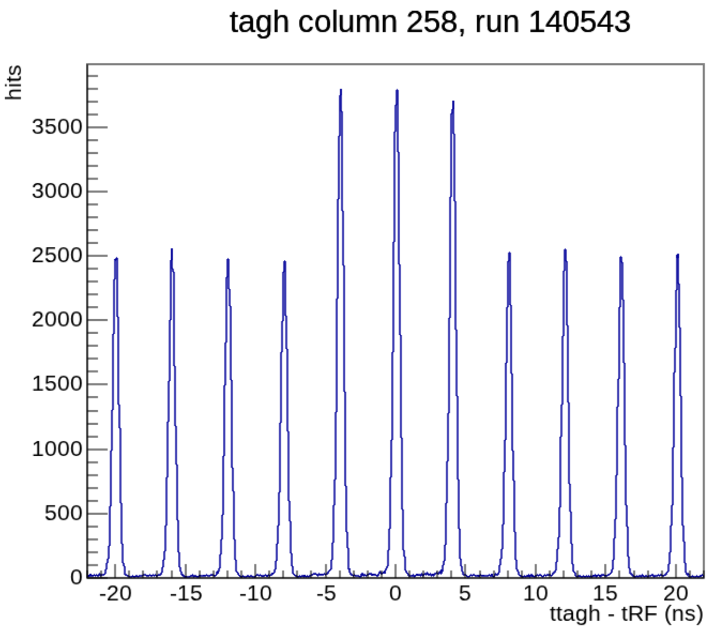

Figure 3: Tag electron hit time distribution relative to the accelerator RF clock for hodoscope counter 258 measured during run 140543 in May, 2026. The enhancement of the three central RF buckets comes from true coincidences with the pair spectrometer located in the bremsstrahlung photon beam downstream of the tagger, which served as the trigger source for the events shown in this plot. The lack of side peaks in the time spectrum for this counter stands in sharp contrast to the hodoscope counters on either side of it.

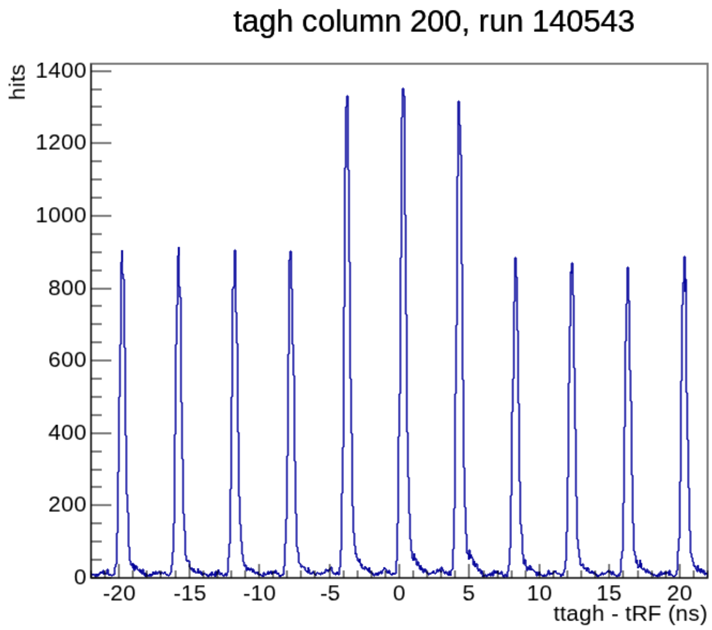

Figure 4: Tag electron hit time distribution relative to the accelerator RF clock for hodoscope counter 200 measured during run 140543 in May, 2026. The enhancement of the three central RF buckets comes from true coincidences with the pair spectrometer located in the bremsstrahlung photon beam downstream of the tagger, which served as the trigger source for the events shown in this plot. The side peaks are visible in this spectrum, but are much smaller than those seen in most counters located closer to the downstream end of the hodoscope.

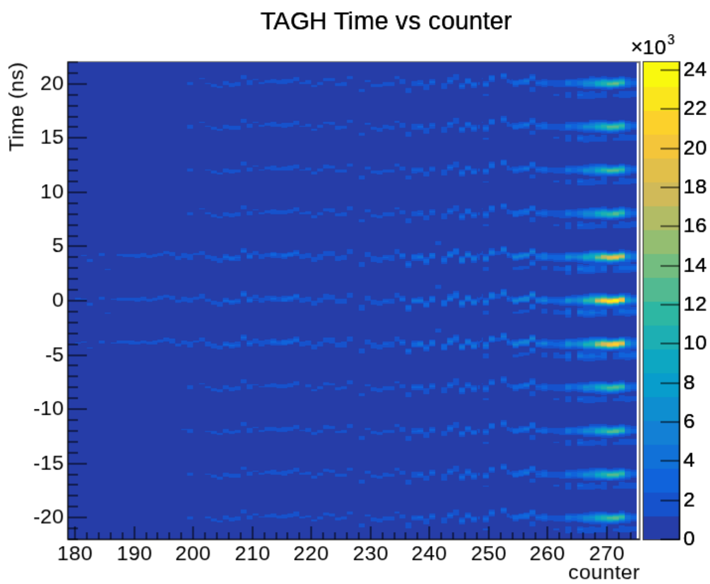

Figure 5: Tag electron hit time distribution relative to the accelerator RF clock versus hodoscope counter number for the full range of the sampling region of the tagger hodoscope during run 140543. The side peaks show up as faint ridges 1 ns below the primary peaks that are regularly spaced every 4 ns.

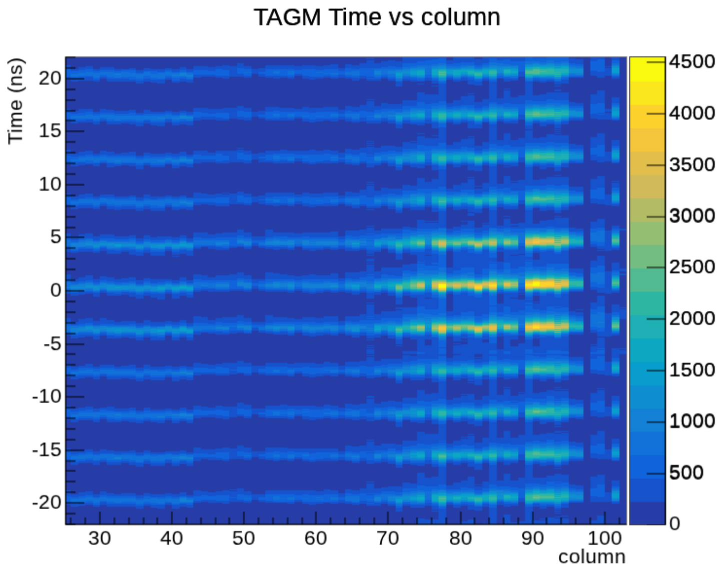

Figure 6: Tag electron hit time distribution relative to the accelerator RF clock versus microscope column number for the downstream end of the tagger microscope during run 140543. The readout of the upstream end of the microscope was not initialized properly during this run, so they are not included in the plot.

the main bunches that arrive every 4 ns. That is not the only possibility to consider, however. One might also imagine that the side peaks are actually delayed by 3 ns, or for that matter by 7 ns or 11 ns, etc., relative to the main peak associated with the same RF beam bucket. In view of the fact that post-bremsstrahlung tag electrons in the main peaks arrive by a fairly direct path that runs for most of its length close to the undegraded electron beam, it would be much easier to imagine how background particles originating from beam interactions somewhere along the beamline might arrive at a focal plane counter later than the post-bremsstrahlung electrons from the same RF beam bucket. Is it possible that each of these side peaks originate from the bunch whose main-peak tags actually arrive 3 ns earlier rather than 1 ns later?

The first piece of evidence that these side-peaks are 1 ns early rather than 3 ns late relative to the main peaks is the relative height of the three side peaks in the middle of Fig. 2. The $t = 0$ time reference in the tagger time spectra is defined by the data acquisition event trigger. In the event sample used for this study, the trigger is generated whenever a coincidence is detected between the right and left arms of the pair spectrometer, indicative of a beam photon undergoing e^+, e^- pair conversion in the thin foil converter located a few meters upstream of the pair spectrometer. The rates in the tagging counters in this region of the focal plane are on the order of 1-2 MHz. At such high rates, there is a high probability that counter 265 will register one or more hits per trigger somewhere in the data acquisition time window, regardless of whether or not the photon that produced the trigger corresponds in energy to this tagging counter. The enhancement of the peaks near $t = 0$ in Fig. 2 comes from events where the energy of the photon that caused the pair trigger actually falls within the range of this tagging counter. The time resolution of the trigger logic circuit is on the order of 10 ns, hence the spread of this enhancement over three adjacent peaks.

The above explanation for the enhancement of the three main peaks near $t = 0$ only strictly applies to the main peaks that contain the post-bremsstrahlung tag electrons. Depending on the origin of the side-peak hits, they may or may not exhibit a similar enhancement due to true coincidences with the photon beam. Examination of the heights of the side peaks in Fig. 2 clearly shows that their event counts rise in proportion to the counts in the main peak that appears immediately afterward delayed by 1 ns, not the ones 3 ns earlier.

While this interpretation of the relative peak heights in Fig. 2 is highly plausible, it is based on assumptions that are difficult to prove, and the above explanation might not be the only one possible. To cross-check this result, a second method was devised to independently identify which side peak shares the same electron beam bucket with which main peak. Each RF bucket in the electron beam contains a slightly different number of electrons, depending on the intensity of the laser pulse that produced it. This shows up in correlations between the accidental hit rates per RF bucket in different tagging counters. For over-populated RF buckets, the probability of a random hit in all tagging counters is slightly higher, and conversely for under-populated buckets. Even if the size of the bucket-to-bucket charge fluctuations are very small, this correlation should be measureable in a sample with large statistics like this run 140543, with positive correlations observed between peaks coming from the same beam bucket in different counters standing out above the uncorrelated peaks associated with different RF buckets. The power of this method arises from the fact that this correlation can be be measured for all possible combinations of peaks for any pair of tagging counters, even those that are located at large distance from one another up and down the focal plane.

Fig. 7 shows the sample statistical correlation between a range of main peaks in tagh counter 100 and the side peaks in tagh counter 265 for run 140543. The fact that the positive correlation shows up for matching peaks in these two widely-separated counters confirms the earlier conclusion that the side peaks come from electrons in the same RF bucket as those in the main peaks just 1 ns later. Note that this correlation would not be observable within just one tagging counter because dead time in the phototube readout forbids detection of hits in both side and main peaks in the same event for the same counter. Fig. 8 shows the same correlation between side peaks in tagh 265 and the main peaks in tagh 200. To confirm that this correlation works as expected for these two pairs of widely separated counters, Fig. 9 shows main peak vs main peak in tagh counters 100 vs 265, and counters 200 vs 265 in Fig. 10. With this cross-check confirmation, the firm conclusion is that whatever is producing these side peaks comes from the same electron bunch as produces the tags in the main peak 1 ns later.

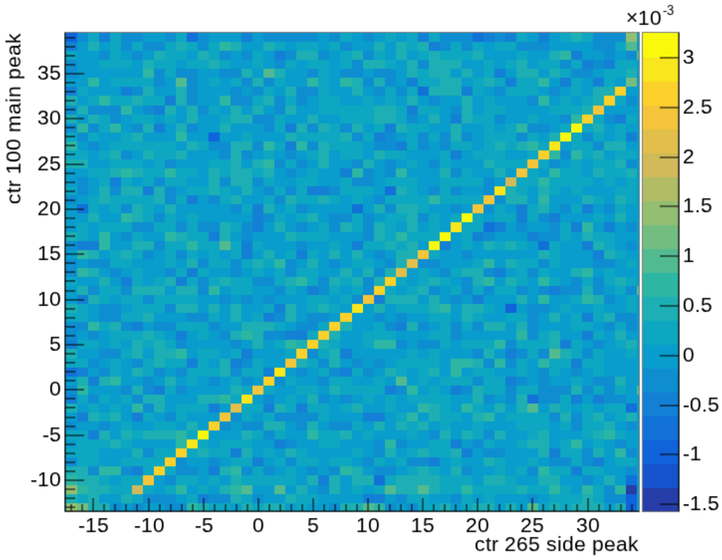

Figure 7: Sample correlation between the per-event hit count in each side peak of the time spectrum from tagh counter 265 and the per-event hit count in each main peak of the time spectrum from tagh counter 100, for run 140543. All pair trigger events in this run are included in this sample. Side peak hits are counted between -1.5 and -0.9 ns of the corresponding main peak center. Main peak hits are counted between -0.3 and +0.3 ns of the main peak center.

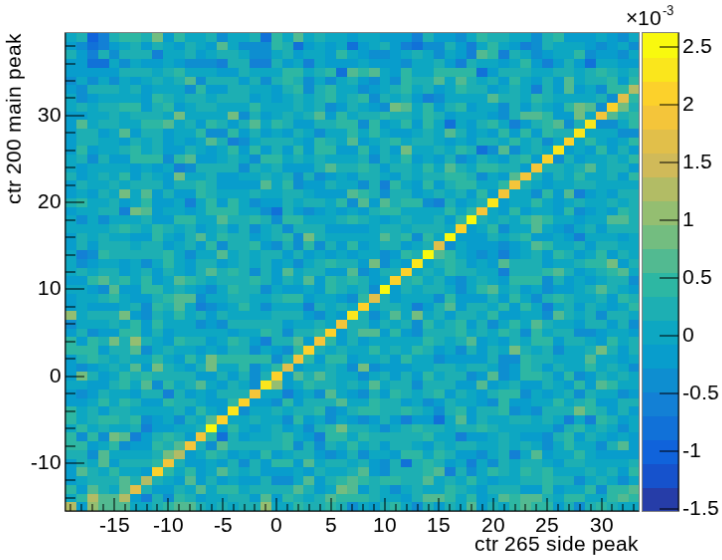

Figure 8: Sample correlation between the per-event hit count in each side peak of the time spectrum from tagh counter 265 and the per-event hit count in each main peak of the time spectrum from tagh counter 200, for run 140543. All pair trigger events in this run are included in this sample. Side peak hits are counted between -1.5 and -0.9 ns of the corresponding main peak center. Main peak hits are counted between -0.3 and +0.3 ns of the main peak center.

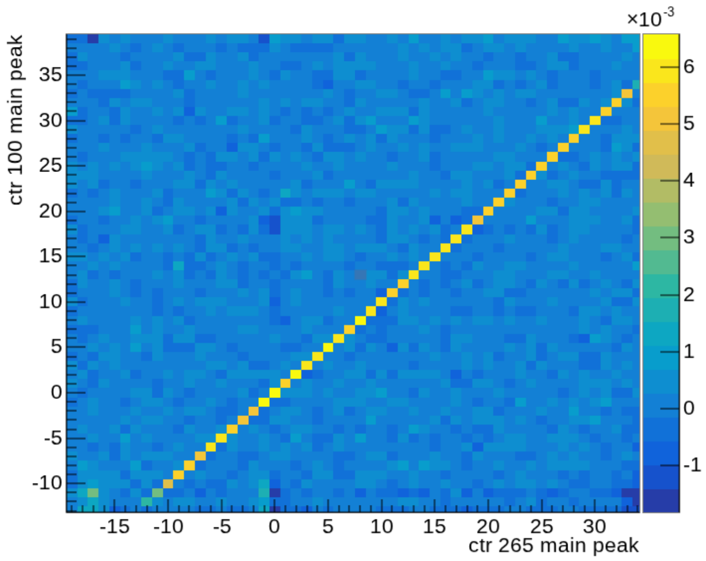

Figure 9: Sample correlation between the per-event hit count in each main peak of the time spectrum from tagh counter 265 and the per-event hit count in each main peak of the time spectrum from tagh counter 100, for run 140543. All pair trigger events in this run are included in this sample. Side peak hits are counted between -1.5 and -0.9 ns of the corresponding main peak center. Main peak hits are counted between -0.3 and +0.3 ns of the main peak center.

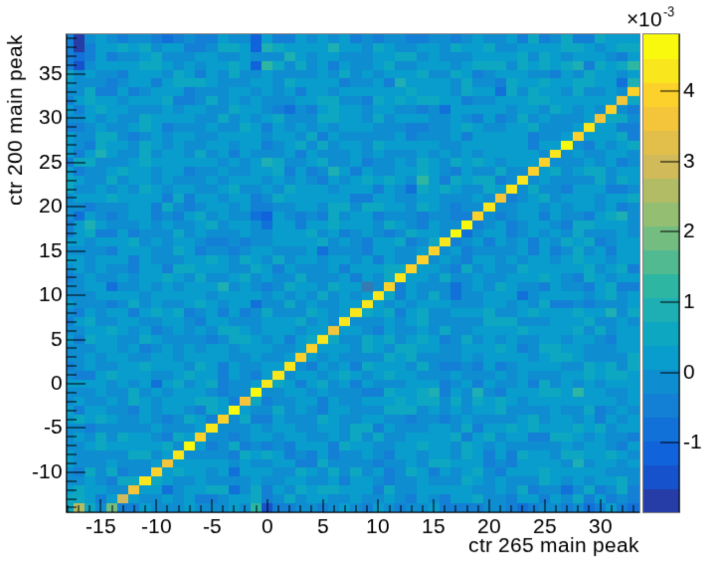

Figure 10: Sample correlation between the per-event hit count in each main peak of the time spectrum from tagh counter 265 and the per-event hit count in each main peak of the time spectrum from tagh counter 200, for run 140543. All pair trigger events in this run are included in this sample. Side peak hits are counted between -1.5 and -0.9 ns of the corresponding main peak center. Main peak hits are counted between -0.3 and +0.3 ns of the main peak center.

3 Considering Möllers as a source

The only one way that an electron from a given RF bunch can reach a focal plane counter before a post-bremsstrahlung tag electron from the same bunch does is by following a shorter path. The path followed by a post-bremsstrahlunch tag electron to a downstream hodoscope counter is illustrated in Fig. 11. The shortest possible path from the diamond radiator to the tagging counters is punching through the vacuum vessel around the radiator target and travelling in a straight line outside the vacuum along the focal plane. The focal plane lies along a radial that passes through the diamond radiator and extends downstream at an angle of 8.7° from the beam axis. Möller electrons from the radiator at this angle have energies close to 45 MeV, as shown in Fig. 12. It is not inceivable that a 45 MeV electron might punch through the goniometer vacuum vessel with sufficient energy to reach the downstream hodoscope counters. Determining whether the Möller rates would be high enough at such a distance from the radiator to produce these peaks is another issue; the first question to answer is whether or not the time difference agrees with this hypothesis given the Hall D tagger geometry.

To answer this question, a simulation was performed to determine the time of flight difference between an electron following the post-bremsstrahlung path shown in Fig. 11 and one following a straight-line path. The result is shown in Fig. 13. This clearly rules out Möllers as a source of the side peaks because there is no way that the time difference of 0.3 ns can stretch far enough to accomodate the measured side-peak separation of 1.2 ns. If one assumes that the Möllers are not coming from the radiator but from some location further upstream along the Hall D electron beamline, the time-of-flight difference can be increased to 0.5 ns, as an absolute upper limit. The explanation of the side peaks as Möller electrons is ruled out.

4 One remaining hypothesis

Apart from positing the existence of tachions, there is only one remaining hypothesis that can explain the observations regarding these timing side-peaks in the tagger hodoscope. They

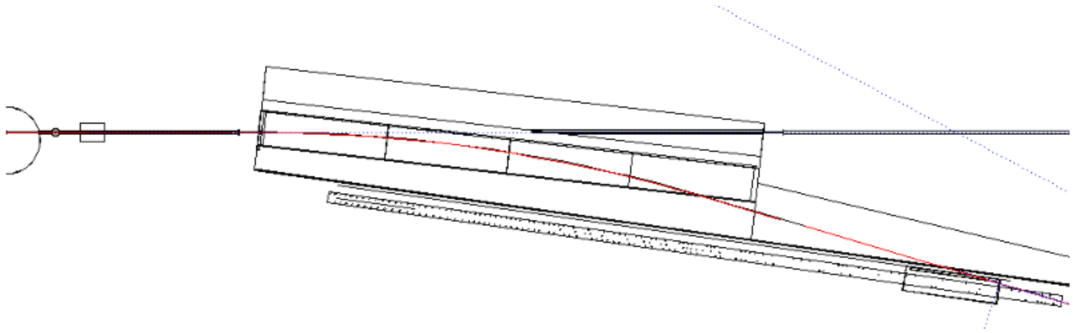

Figure 11: Horizontal slice through the Hall D tagger at the beam elevation, with the radiator crystal in its vacuum chamber at the left side of the figure, and the electron beam exiting the tagger toward the beam dump toward the lower right. The red curve is the track of a post-bremsstrahlung electron that radiates a photon at the radiator and gets bent in the spectrometer into the focal plane of the tagger. The figure was produced by the Geant simulation of the Hall D tagger and beamline.

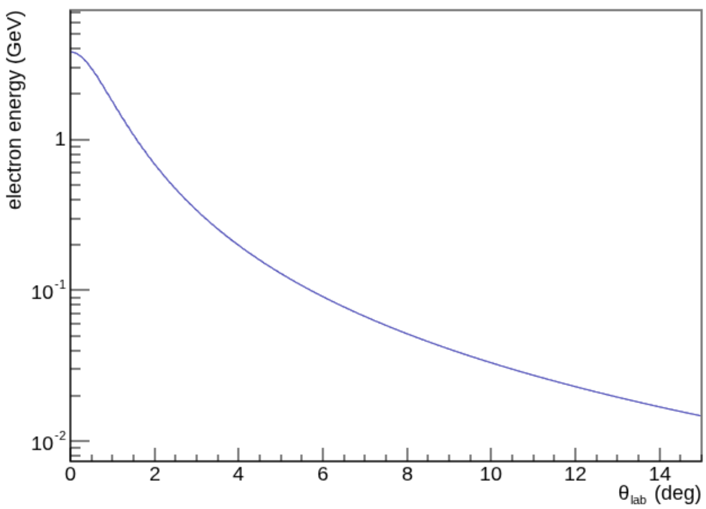

Figure 12: Möller kinematics for a 3.8 GeV electron beam, showing the total energy of one of the final-state electrons as a function of lab polar angle.

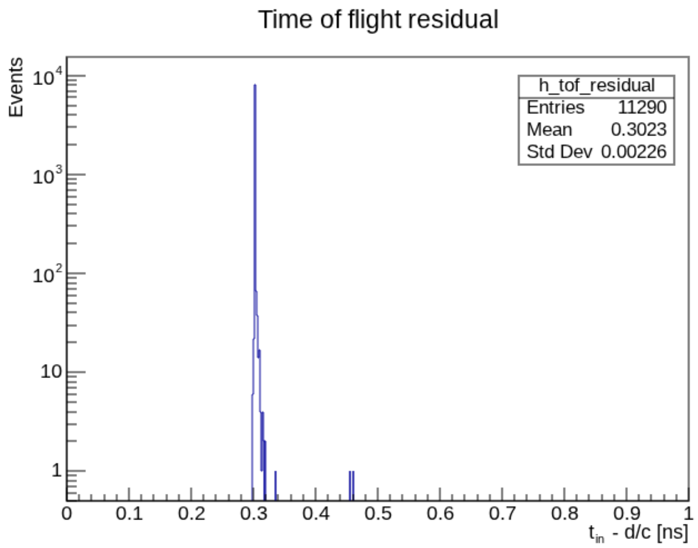

Figure 13: Time-of-flight difference between an ordinary post-bremsstrahlung electron that radiates a photon in the radiator, and gets steered in the tagger dipole field into a tagging counter, with a Möller electron that travels along a straight-line path from the radiator to the same tagging counter. The small spread in these values takes into account the beam emittance, angular spread in the bremsstrahlung emission and multiple scattering in the radiator.

must come from impacts of electrons directly in the walls and/or electrodes of the hodoscope counter photomultipler tubes. The Hall D tagger hodoscope counters are constructed with the scintillators glued directly to the photocathode window of the phototube without any use of light guides. If a post-bremsstrahlung electron or one of its secondaries strikes the phototube either directly on the phototube or near its first dynode and showers, it could plausibly inject as many enough secondary electrons at the start of the dynode chain as would a light pulse from the scintillator. Although the arrival time of the post-bremsstrahlung electron or shower secondary would be the same whether it interacted in the scintillator or in the walls of the phototube, the rise-time of the scintillator light pulses would be slowed by the scintillator fluorescence decay lifetime on the order of 2 ns. This might easily account for the time difference of 1.2 ns between the scintillator and the glass-shower interactions.

The following three predictions, made on the basis of this hypothesis, permit it to be empirically tested. If this hypothesis is correct, then

1. the two charge creation mechanisms are different, so the pulse height distributions should not match;
2. the pulse shapes should be different, with the side peaks having faster rise times than the main peaks by roughly 2 ns;
3. the phototubes sit well above the post-bremsstrahlung scattering plane, so most of what hits directly on the walls of the phototubes must be coming from showers of post-bremsstrahlung electrons in the poles of the spectrometer. The random spray from these showers would mean that the side-peak tags should not show as strong a tagging correlation between the tagging counter number and the energy of beam photons from the same RF bucket as is seen for main-peak tags.

4.1 pulse height comparison

The raw pulse height distributions for the main peaks (red) and side peaks (blue) are shown in the open histograms of Fig. 14. Clearly they are different both in mean value and in width.

The contrast becomes more stark after accidentals are subtracted, as shown for the main-peak hits by the solid red histogram. The side peaks do not show any significant difference between the pulse height distributions for true and accidental coincidences with the pair spectrometer, whereas for true tags in the main peaks, the pulse height distribution is much more narrow and smaller in magnitude.

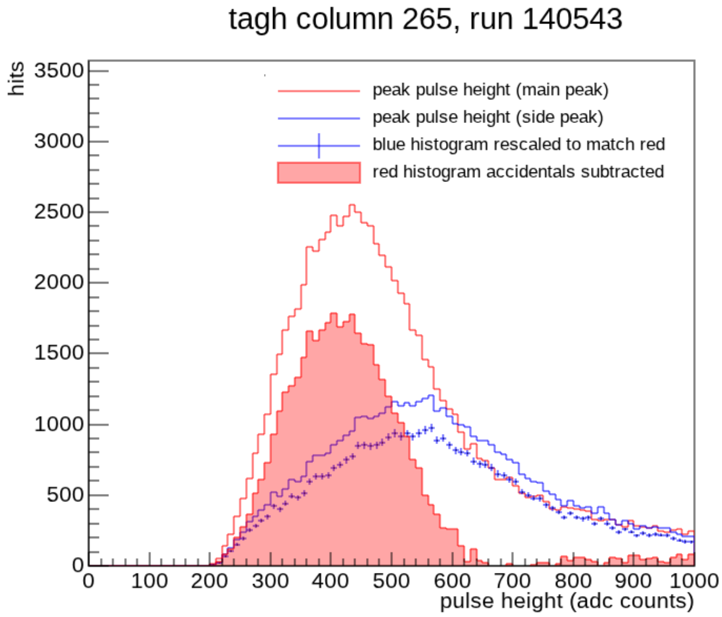

Figure 14: Pulse height distributions for hits in tagh counter 265 based on GlueX data collected in run 140543 in May, 2026. The open histograms show the raw distributions for hits in the main peaks (red) and the side peaks (blue). The solid red histogram results when accidental coincidences with the pair spectrometer are subtracted. Accidentals subtraction in the case of the side peaks does not change the shape of the distribution.

4.2 pulse shape comparison

The reason that this one run 140543 was chosen for this study is that it was taken with the data acquisition in operating in raw pulse readout mode. This means that the complete waveforms for each hit in the tagging counters were written to the data stream. By putting together the waveforms from a large number of pulses from the same electronics channel, and normalizing each one to the same pulse height, a high-resolution picture of the phototube pulse from the tagger hodoscope is formed. Fig. 15 shows the result for tagh counter 265 where only pulses from the main peaks are included. The corresponding waveform for just the side-peak hits from tagh counter 265 is shown in Fig. 16. Taking the fitted sigma from the central region of the peak as to estimate the rise time, the side peaks show a faster rise by by 2 ns, as expected under the working hypothesis.

For completeness, a reconstructed waveform is included for one of the channels in the microscope in Fig. 17. Similarly for the pair spectrometer, reconstructed pulse shapes for a typical channel in the pair spectrometer fine-structured array is shown in Fig. 18 and for the pair spectrometer coarse-structured array in Fig. 19. Four-fold coincidence between a fine and coarse counter on the left arm and a fine and coarse counter on the right arm are required by the pair spectromter trigger.

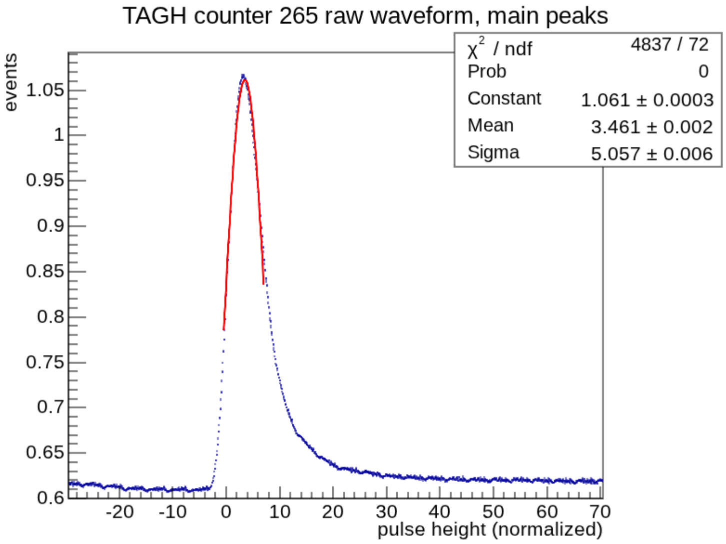

Figure 15: Raw signal waveform of pulses in the main peaks for tagh counter 265, reconstructed from the raw adc waveforms recorded by the data acquisition during run 140543. The parameters are the results of a gaussian fit to the restricted region around the peak maximum.

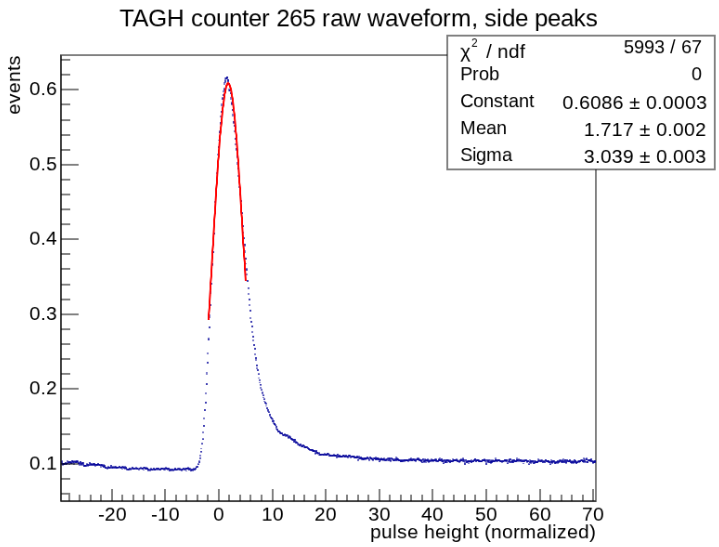

Figure 16: Raw signal waveform of pulses in the side peaks for tagh counter 265, reconstructed from the raw adc waveforms recorded by the data acquisition during run 140543. The parameters are the results of a gaussian fit to the restricted region around the peak maximum.

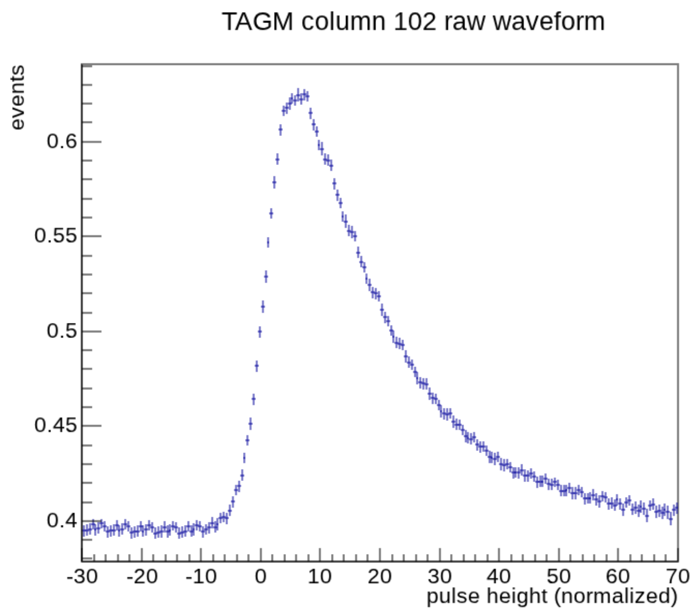

Figure 17: Raw signal waveform of pulses in tagger microscope column 102, reconstructed from the raw adc waveforms recorded by the data acquisition during run 140543. Pulses from the silicon photomultipliers in the tagm readout are somewhat slower than the photomultiplier tube pulses from the tagh counter readout.

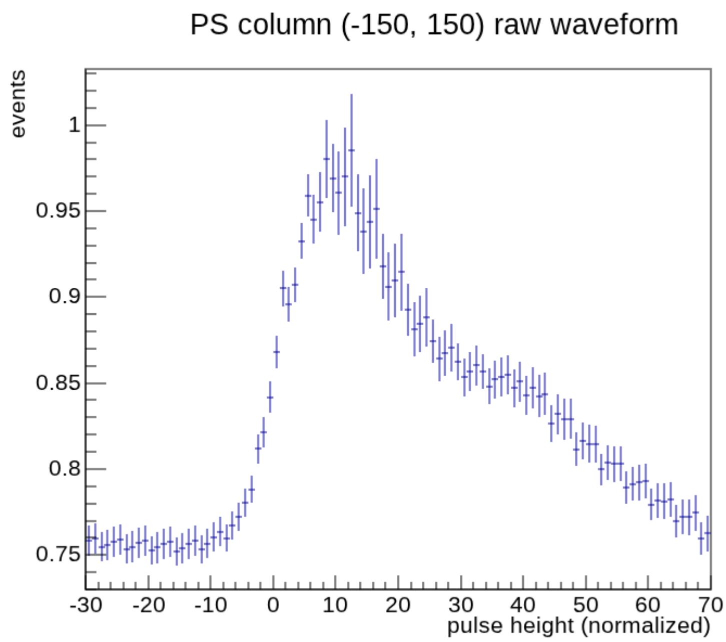

Figure 18: Raw signal waveform of pulses from one of the fine-structure array counters in the pair spectrometer. The width of these pulses arises from the silicon photomultiplier readout of the pair spectrometer fine counters.

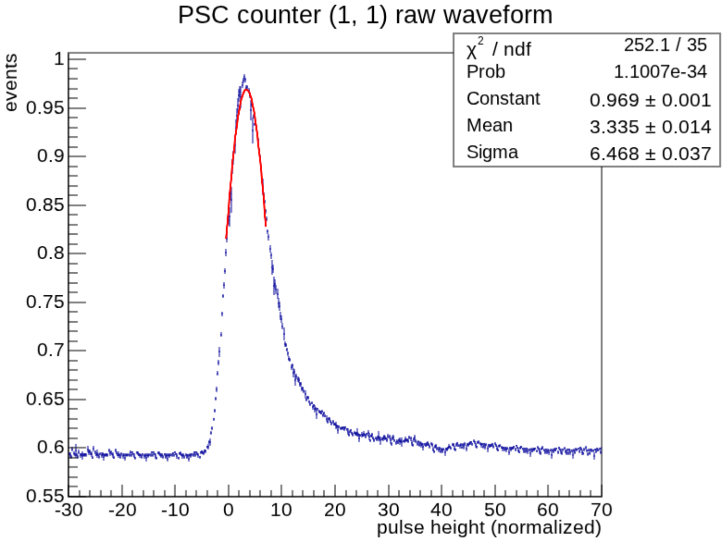

Figure 19: Raw signal waveform for hits from one of the coarse-structure array counters in the pair spectrometer. The coarse counters in the pair spectrometer are read out with photomultiplier tubes for optimum time resolution.

4.3 tagger energy resolution comparison

4.4 Data Tables

Table 1 presents the primary experimental run parameters and measured outputs using the `booktabs` package.

Table 1: Summary of experimental runs and key measured values.

Run ID	Beam Energy (GeV)	Target Mass (u)	Cross Section (pb)
Run 101	8.5	1.008	12.4 ± 0.3
Run 102	9.0	1.008	15.1 ± 0.4
Run 103	12.0	4.002	42.8 ± 1.1

Acknowledgments

This work is supported by the U.S. National Science Foundation under grant 2514864.

References

[1] A. Author and B. Coauthor, *Journal of Scientific Examples*, vol. 42, no. 3, pp. 100–110, 2026.

[2] Calibration Constants Database (CCDB) Documentation, https://ccdb.example.org/docs. *Comprehensive user guide and API reference detailing database schema versions, user access controls, and calibration parameter updates for experimental setups.* (Accessed: August 2026).

[3] JANA2 Multi-threaded Analysis Framework. *Official documentation for the C++ multi-threaded data processing framework used for high-energy physics event reconstruction and parallel data analysis pipeline execution.*